Proceedings of the 2003 IEEE/RSJ
Intl. Conference on Intelligent Robots and Systems
Las Vegas, Nevada · October 2003

Towards Optimal Coverage of 2-Dimensional Surfaces Embedded in $I\!R^3$: Choice of Start Curve

Prasad N. Atkar Howie Choset Alfred A. Rizzi
Carnegie Mellon University, Pittsburgh, PA 15213
atkar@cmu.edu choset@cmu.edu arizzi@ri.cmu.edu

***Abstract*— For automated spray painting robots, the choice of a start curve from which all subsequent paths will be determined, plays a critical role in ensuring uniform coverage of the target surface. In this paper, we ultimately propose a method to determine the start curve for two different procedures of coverage path construction. For the first procedure, we average the target surface normal to optimize the average error between desired and resultant deposition with the added goal of minimizing cycle time. For the second technique, we make recourse to the Gauss-Bonnet theorem to minimize the non-uniformity of paint deposition and cycle time for the entire coverage path.**

I. Introduction

The automobile market demands a uniform deposition of paint on car body surfaces (*uniformity optimization*), whereas the manufacturer seeks minimal cycle time for economic manufacturing (*cycle time optimization*). To meet these optimization criteria, we develop a new algorithm to generate a *coverage path* from a finite number of curves termed *passes* on the target surface. The spacing between adjacent passes is termed as the *inter-pass* distance.

Prior literature review and our experience suggests that there are two basic approaches to generate passes in a coverage path. The first, a *section plane planner*, generates passes by intersecting the target surface with a series of parallel equidistant planes termed *section planes* (see Figure 1(a)). The second, an *offset curve planner*, first generates a *start curve* on the target surface, then constructs the subsequent passes by offsetting the start curve along a family of curves orthogonal to the start curve (see Figure 1(b)). For both the planners, choosing a start curve (or the section plane) and determining the optimum spacing between adjacent passes completely specifies the coverage path.

We have performed simulations of paint deposition on a door panel from a Ford Excursion to verify the significance of the choice of a start curve on uniformity and cycle time (see Figure 2). Using an offset curve planner, we constructed the coverage paths for the surface using different start curves. Even though we used the same spacing (measured along the orthogonal curves) between adjacent passes for both the coverage paths, these coverage paths yielded different paint deposition uniformity (measured in terms of normalized std. deviation of the paint deposition) as well as different cycle times. Thus, we conclude that the choice of the start curve is critical for coverage tasks that must meet the uniformity and cycle time goals.

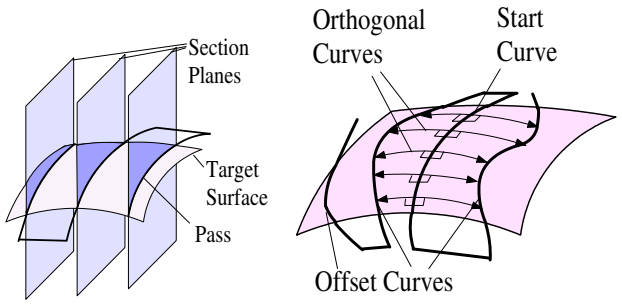

Fig. 1. Coverage path construction using (a) section planes (b) offset curves.

In this paper, we provide a technique that determines the start curve by solving the constrained optimization problem involving uniformity and cycle time goals. Our method is applicable for both approaches of coverage path construction. Our focus is only on the selection of a start curve, and we assume that we already have a mechanism to determine the optimal spacing between adjacent passes.

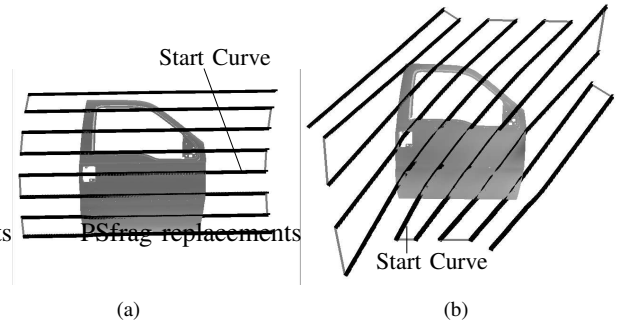

Fig. 2. Simulated coverage paths on a Ford Excursion door: choice of different start curves yields different uniformity and cycle time. The normalized std. deviation for paint deposition is 9.02% for (a) and 10.44% for (b). The number of turns in the coverage paths for in (a) and (b) are 8 and 10 respectively, thus suggesting shorter cycle time for (a).

II. Prior Work

Most of the prior automated path planning algorithms for material deposition or removal tasks focus on robotic spray painting and CNC machining respectively. Among the prior efforts that optimize the uniformity of material deposition (removal), most focus on determining the optimal spacing between the adjacent passes. For CNC ball-end cutter milling applications, the uniformity of material removal is measured in terms of the maximum error between the machined surface and the design surface, termed the *scallop height*. Suresh and Yang [1] determine optimal spacing between adjacent passes to ensure constant scallop height. Sarma and Dutta [2] generalize this technique to control a given distribution of scallop height, including the constant scallop height distribution. Determining the optimal inter-pass spacing for robotic spray painting [3], [4], [5], [6] is relatively more involved due to the complexity of the paint distribution flux coming out of the spray gun [7].

Prior research has not focused on techniques to determine the optimal start curve, although the choice is critical in improving the uniformity of deposition and reducing the cycle time. Prior results depend on the user selecting a start curve [2], or choose a boundary curve [1] as a start curve. Other methods use bounding box methods [3], [4], [5], [6] to determine the pass orientation and the offset-direction.

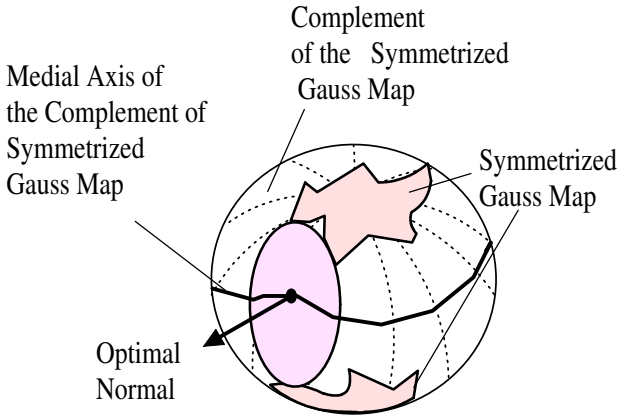

Fig. 3. Optimal section normal as the center of the largest circle inscribed in the compliment of the symmetrized Gauss map of the target surface.

One notable result in the CNC literature selects the optimal section plane normal for use in a section plane planner. In [8] Smith *et al.* compute the optimal orientation of the section plane normal as the vector that is maximally "away" from the normals to the surface to minimize the maximum scallop height. For a section plane planner determining this orientation (as well as the position) of the section planes is analogous to selecting the start curve.

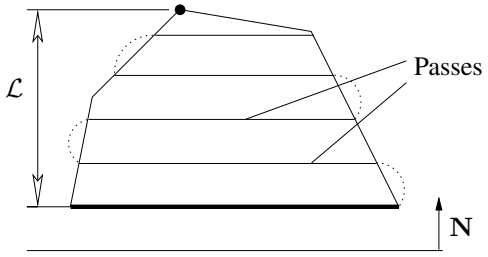

Fig. 4. The number of passes in coverage path for the planar polygon will be minimized when the passes are parallel to one of the edges for a fixed spacing between adjacent passes.

Their method maintains the optimal spacing between adjacent passes by using a constant spacing between adjacent planes and making the section planes as orthogonal as possible to the target surface. They accomplish this by choosing the normal to the section planes as the unit vector corresponding to the center of the largest circle inscribed in the complement of the symmetrized Gauss map of the target surface (see Figure 3).

The choice of section plane normal in Smith's method is highly sensitive to small changes in the target surface which may cause large changes in the Gauss map. Such changes may result in a significant increase in the *average* scallop height over the surface, even though the *maximum* scallop height remains approximately the same. For example, the image of the Gauss map of a large planar sheet is a single point. If this sheet is rolled a little near its edges to form cylindrical and spherical extensions, the general geometry of the surface remains the same in comparison to the geometry of the deposition pattern. Yet the Gauss map of this slightly deformed sheet changes significantly thus producing a significantly different optimal section plane normal and consequently a significantly different coverage path.

Apart from affecting deposition uniformity, the choice of start curve significantly impacts the cycle time due to its effect on the number of passes and their lengths in a coverage path. Particularly, for the painting application, cycle time depends significantly on the number of turns in the coverage path. For polygons (possibly with polygonal holes), Huang [9] optimizes the cycle time by reducing the number of turns in a coverage path. His approach minimizes the "height" $\mathcal{L}$ of the polygon in the direction $\mathbf{N}$ orthogonal to the orientation of the passes (see Figure 4). This height is directly proportional to the number of passes and is minimized when the orientation of the passes is parallel to one of the polygon's edges.

Unfortunately, all the prior work discussed here seeks to optimize either the uniformity of deposition (removal) or the cycle time. None of the techniques address the simultaneous optimization of both, which is critical to majority of real world applications.

III. Choice of the Start Curve for Offset Curve Planner

The offset curve planner (see Figure 1(b)) generates a start curve on the surface and then offsets it along a family of curves orthogonal to the start curve. The geodesic curvature of the start curve and the offset curves has significant impact on the uniformity of material deposition (Sarma and Dutta [2]). This is because a high geodesic curvature of the offsets may result in self-intersections of subsequent offsets, even for small offset distances. Self intersections lead to tangent discontinuities on offset curves rendering the robot end effector motion infeasible and severely hampering the uniformity.

We analyze the geodesic curvature of the offset curves for arbitrary start curves in Section III-A, and conclude that the start curve should be a geodesic. However, there are infinitely many choices for the starting geodesic curve on the target surface. In Section III-B, we use the notion of a Gaussian curvature divider to select a particular set of geodesics to improve the deposition uniformity.

A. Properties of Offset Curves and Their Implications

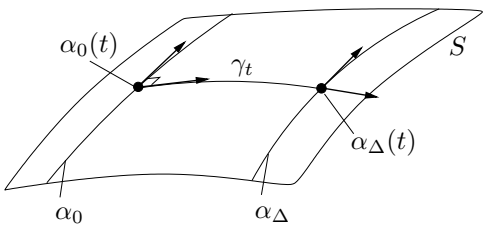

Fig. 5. Geodesic offsets are defined by moving the start curve "sideways" (here, to the right) along the orthogonal geodesics.

First, let us consider the offset curve planner, where offsetting is done along unit speed geodesics orthogonal to the start curve. In Figure 5, α_0 is a start curve parametrized by t on surface S. At any given point $\alpha_0(t)$ along α_0, let $\gamma_t(s)$ be a geodesic starting at $\alpha_0(t)$ and orthogonal to α_0. In other words, $\frac{d\gamma_t(0)}{ds} \perp \frac{d\alpha_0(t)}{dt}$. Since, these geodesics are parametrized by arc-length (unit speed), $\gamma_t(\Delta)$ represents a point on surface S at geodesic distance Δ from point $\alpha_0(t)$. Then the geodesic offset of curve $\alpha_0(t)$ at the geodesic distance Δ is defined as

$$\alpha_\Delta(t) = \gamma_t(\Delta). \tag{1}$$

Rausch *et al.* [10] have studied the properties of geodesic offsets for computation of medial axis on curved surfaces. They define the *focal point* of a start curve α_0 as the point on the offset curve α_s where $\frac{d\alpha_s(t)}{dt} = \mathbf{0}$. The smallest offset distance δ for which the focal point appears on the offset curve α_δ, is termed the *focal length* of start curve α_0. If the offset distance exceeds the focal length of the start curve, self-intersections will appear on the offset curve.

If the offset distance, s, is less than the focal length of the start curve, Rausch *et al.* show the following important properties of geodesic offset curves

$$\frac{d\gamma_t(s)}{ds} \perp \frac{d\alpha_s(t)}{dt}, \tag{2}$$

$$\frac{d^3(\alpha_s(t))}{ds^2 dt} + K(\alpha_s(t))\frac{d(\alpha_s(t))}{dt} = 0, \quad \text{and} \tag{3}$$

$$\frac{d^2(\alpha_s(t))}{ds dt} + \kappa_g(\alpha_s(t))\frac{d(\alpha_s(t))}{dt} = 0, \tag{4}$$

where $K(p)$ denotes the Gaussian curvature at point $p \in S$, and $\kappa_g(\beta(t))$ denotes the geodesic curvature of a curve $\beta \in S$ at $\beta(t)$. Note that the derivatives $\frac{d^2(\alpha_s(t))}{ds^2}$ and $\frac{d(\alpha_s(t))}{ds}$ are calculated along the orthogonal geodesic $\gamma_t(s)$ at the point $\alpha_s(t) = \gamma_t(s)$.

From (3) and (4), it is clear that the geodesic curvature of the offset curve depends both on the geodesic curvature of the start curve and the Gaussian curvature of the surface. Two important consequences of this are: 1) There will always be self intersections on the offset curves, if the start curve is not a geodesic and the target surface has zero Gaussian curvature [1] everywhere. 2) The offsets of a geodesic start curve will not be geodesics in general on surfaces with non-zero Gaussian curvature. Thus, there is more probability that an offset curve will self-intersect on a curved surface.

These facts suggest that the minimization of the geodesic curvature decreases the probability of self intersections of offset curve. Thus, we conclude that the geodesic curvature of the offset curves should be minimized to improve deposition uniformity. Another obvious consequence is that the start curve should be a geodesic to minimize the integral of geodesic curvature of the offset curves.

B. Choosing Start Curves as Geodesics: Application of Gauss Bonnet Theorem

There are infinitely many geodesics passing through each point on the surface. Our task is to select the geodesic start curve that minimizes the geodesic curvature of the subsequent offset curves. Here, we make recourse to the Gauss-Bonnet Theorem and provide a method to minimize the integral of geodesic curvature along the offset curves.

Let us consider a segment C_{st} of the smooth start curve α_0 (see Figure 6). Let the end-points of C_{st} be $\alpha_0(t_0)$ and $\alpha_0(t_1)$. Let C_{of} be the offset of curve C_{st} along α_Δ with endpoints $\alpha_\Delta(t_0)$ and $\alpha_\Delta(t_1)$, where Δ is less than the focal length of α_0. We are interested in determining the integral of the geodesic curvature along C_{of}. Let γ_{t_0} and

[1] plane, surfaces of linear extrusion, cone etc.

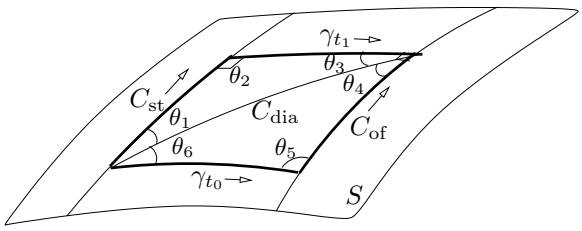

Fig. 6. Application of Gauss Bonnet Theorem to region bounded by the start curve, its offset curve, and the two bounding orthogonal geodesics.

γ_{t_1} be the orthogonal geodesics to curve α_0. We assume that the surface is C^3 continuous, therefore α_Δ, γ_{t_0} and γ_{t_1} are all smooth curves.

Let ϕ be the region bounded by $C_{\rm st}$, $C_{\rm of}$, γ_{t_0} and γ_{t_1}. Let $C_{\rm dia}$ be any smooth curve joining $\gamma_{t_0}(0)$ and $\gamma_{t_1}(\Delta)$. Let us denote the surface region bounded by $C_{\rm st}$, γ_{t_1} and $C_{\rm dia}$ as ϕ_1. Clearly, its boundary $\partial\phi_1$ consists of curves $C_{\rm st}$, γ_{t_1} and $C_{\rm dia}$ with appropriate orientation. Similarly, let ϕ_2 be the region bounded by $C_{\rm of}$, γ_{t_0} and $C_{\rm dia}$, and $\partial\phi_2$ be the boundary of ϕ_2.

Applying the local Gauss Bonnet Theorem (Thorpe [11]) to regions ϕ_1 and ϕ_2, it follows that

$$\int_{\phi_1} K + \int_{\partial\phi_1} \kappa_g = (\theta_1 + \theta_2 + \theta_3) - \pi, \tag{5}$$

$$\int_{\phi_2} K + \int_{\partial\phi_2} \kappa_g = (\theta_4 + \theta_5 + \theta_6) - \pi. \tag{6}$$

The integrals $\int_{\gamma_{t_0}} \kappa_g$ and $\int_{\gamma_{t_1}} \kappa_g$ are zero by definition of geodesics. Therefore,

$$\int_{\partial\phi_1} \kappa_g + \int_{\partial\phi_2} \kappa_g = \int_{C_{\rm st}} \kappa_g - \int_{C_{\rm of}} \kappa_g. \tag{7}$$

Note that the terms containing $\int_{C_{\rm dia}} \kappa_g$ cancel because the curve is traced in opposite directions each time.

Also note that $\int_{\phi_1} K + \int_{\phi_2} K = \int_{\phi} K$. Applying these results to the summation of (5) and (6), it follows that

$$\int_{\phi} K + \int_{C_{\rm st}} \kappa_g - \int_{C_{\rm of}} \kappa_g \quad = \quad (\theta_1 + \theta_6) + \theta_2 + (\theta_3 + \theta_4) + \theta_5 - 2\pi. \tag{8}$$

Since $\theta_1 + \theta_6 = \theta_2 = \frac{\pi}{2}$ and $\theta_3 + \theta_4 = \theta_5 = \frac{\pi}{2}$ by (2), it follows that expression (8) is identically zero. Then rearranging, we can write

$$\int_{C_{\rm of}} \kappa_g = \int_{\phi} K + \int_{C_{\rm st}} \kappa_g. \tag{9}$$

And finally, if the start curve is a geodesic, then

$$\int_{C_{\rm of}} \kappa_g = \int_{\phi} K. \tag{10}$$

Our goal is to minimize the integral of the geodesic curvature over the offset curve. Let C_l and C_h be the last passes on the surface on either side of start curve α_0. Then, if ϕ^- is the region bounded between C_l and α_0, $\int_{C_l} \kappa_g = \int_{\phi^-} K$. Similarly, if ϕ^+ is the region bounded between C_h and α_0, $\int_{C_h} \kappa_g = \int_{\phi^+} K$. Then, $\int_{C_l} \kappa_g + \int_{C_h} \kappa_g = \int_{\phi^-} K + \int_{\phi^+} K \approx \int_S K$, which is a constant. Note that the approximation in the expression is due to the fact that the last offset curves C_h and C_l do not necessarily lie on the surface boundary and thus $\phi^- \cup \phi^+$ does not exactly cover S. Then, it is easy to see that the maximum between $\int_{C_l} \kappa_g$ and $\int_{C_h} \kappa_g$ is minimized when $\int_{\phi^-} K = \int_{\phi^+} K$.

Thus, the integral of geodesic curvature on the offset paths is minimized when the start curve α splits the surface S into two disjoint regions ϕ^- and ϕ^+ such that $\int_{\phi^-} K = \int_{\phi^+} K = \frac{1}{2}\int_S K$. Such a curve is termed *Gaussian curvature divider*.

The analysis in this Section does not require the start curve to be a geodesic, it merely concludes that the start curve should be a Gaussian curvature divider. Recall that the conclusion from Section III-A suggested that the start curve should have low geodesic curvature. That is, the start curve should preferably be a geodesic. Thus, combining the results from this Section and Section III-A, we conclude that the start curve should be a geodesic Gaussian curvature divider.

For practical implementation, we have observed that the use of geodesics as start curves often lead to intersection between of the path extensions used for overspray. To the contrary, when curves obtained by intersecting the target surface with an orthogonal plane are used as the start curve, the quality of overspray extensions in the coverage path is better (no intersections). These curves of planar intersection are close to being geodesic, therefore the geodesic curvature analysis in this Section and Section III-A applies to this family of planar curves within reasonable limits. Therefore, for practical implementation, we determine the start curve as a planar intersection curve that is also a Gaussian curvature divider. There are multiple planar intersection curves which are Gaussian curvature dividers; we will select one that minimizes the cycle time in Section IV-C.

IV. Choice of the Optimal Start Curve for Section Plane Planner

The choice of the optimal start curve for the section plane planner (Figure 1(a)) to meet uniformity and cycle time goals has two subproblems: choice of the position of the section plane (distance from origin) used for generating the start curve and choice of the orientation of the plane. In Section IV-A, we determine feasible orientations for section plane normal for uniformity criterion and then choose optimal section plane normal from this feasible set that optimizes cycle time in Section IV-B. Finally, we determine the optimal start curve in Section IV-C.

A. Choice of Section Plane Normal for Uniformity Goal

We determine the optimal section plane normal to maximize uniformity based on ideas of Smith *et al.* [8]. Their method minimizes the maximum scallop height but yields a non-optimal average scallop height. To minimize the average error between actual and desired deposition levels, we consider section normals orthogonal to the *average surface normal*. Following the analysis of Smith *et al.*, we conclude that, in general, the section plane normals that are orthogonal to the averaged (weighted) surface normal will yield acceptable scallop heights and equivalently acceptable deposition (removal) uniformities. This approach of averaging the target surface normal has a major added benefit, namely, the ability to optimize for the cycle time over section plane normals that meet the uniformity goal.

We compute the average target surface normal directly on the target surface by integrating the surface normal over the entire surface. The average surface normal $\mathbf{n}_{\text{avg}}$ for surface S is given by

$$\mathbf{n}_{\text{avg}} = \frac{\int_S \mathbf{n}_s}{||\int_S \mathbf{n}_s||}, \tag{11}$$

where $\mathbf{n}_s$ is the surface normal at a point $s \in S$. Then, the set of section plane normals orthogonal to the averaged surface normal is

$$\mathcal{N}_{\text{uni}} = \{N : N \in \mathsf{S}^2, \langle N, \mathbf{n}_{\text{avg}} \rangle = 0, N \nparallel \mathbf{n}_s \ \forall s \in S\}. \tag{12}$$

Note that the restriction $N \nparallel \mathbf{n}_s$ ensures that the section plane normal is not parallel to the surface normal at any point, and the scallop height stays within acceptable levels. If $\mathcal{N}_{\text{uni}}$ were an empty set, then the target surface curves so much that any section plane chosen becomes tangent to the target surface at some point. This in turn implies poor deposition (removal) uniformity no matter which section plane is chosen.

B. Cycle Time Minimization for Section Plane Planner

Note that the set $\mathcal{N}_{\text{uni}}$, in general,forms a great circle on the unit sphere (used to represent the Gauss map of the surface). Therefore, there are infinitely many choices for the section plane normals that meet the uniformity criterion. Here, our objective is to determine the section plane normal that minimizes the cycle time over the set of normals meeting uniformity criterion, that is, $\mathcal{N}_{\text{uni}}$. The cycle time depends strongly on the number of turns in the coverage path, therefore we seek to minimize number of turns.

We extend Huang's [9] analysis to curved surfaces embedded in $\mathbb{R}^3$ to minimize the number of passes in the coverage path. To compute the number of passes in a coverage path, we first determine the "width" of the surface along the section normal. Let us assume that

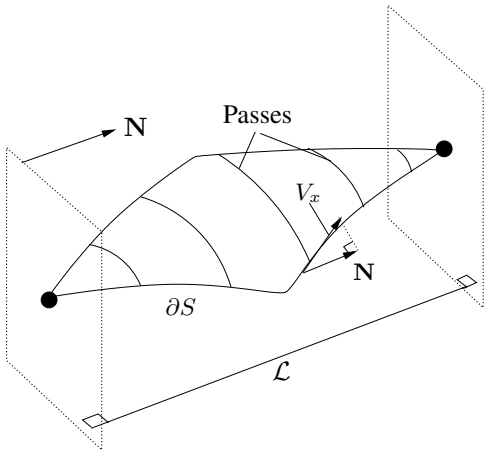

Fig. 7. The number of passes in the coverage path for section plane orientation $\mathbf{N}$ is directly proportional to the width $\mathcal{L}$ of the surface S along $\mathbf{N}$.

we generate the coverage path by intersecting the target surface with a series of section planes with normal $\mathbf{N}$ and interplanar distance Δ. Let the target surface S be a surface patch with boundary ∂S. Let $V_x \in T_x \partial S$ be a unit vector tangent to the oriented boundary ∂S at a point $x \in \partial S$ (see Figure 7). Then, the width $\mathcal{L}$ of the target surface along the section normal $\mathbf{N}$ is given by

$$\mathcal{L}(\mathbf{N}) = \frac{1}{2} \int_{\partial S} |\langle \mathbf{N}, V_x \rangle| dx. \tag{13}$$

Then, the number of passes in the coverage path is given by

$$\mathcal{P}(\mathbf{N}) = \text{ceil}\left(\frac{\mathcal{L}(\mathbf{N})}{\Delta}\right). \tag{14}$$

Thus, we can determine the number of passes in a coverage path obtained by using section normal $\mathbf{N}$. We determine the optimal section plane normal $\mathbf{N}^*$ that minimizes cycle time (the number of turns) over $\mathcal{N}_{\text{uni}}$ as

$$\mathbf{N}^* = \{\mathbf{N} \in \mathcal{N}_{\text{uni}} : \mathcal{P}(\mathbf{N}) \leq \mathcal{P}(N), \ \forall N \in \mathcal{N}_{\text{uni}}\}. \tag{15}$$

Since $\mathcal{P}$ is an integer function, its minimum will generally not be unique; thus there could be multiple normals in $\mathcal{N}_{\text{uni}}$ that satisfy this criterion equally well. Then, we apply Smith's criterion to the normals in the set $\mathbf{N}^*$, that is, we select the normal from $\mathbf{N}^*$ whose distance from the boundary of the Gauss map is maximum as the optimal normal.

C. Determining the Optimal Start Curve

Now that we have defined the orientation of the section plane that yields the start curve as $\mathbf{N}^*$, we want to determine its distance from the origin to completely specify the start curve. In this Section, we derive a result that finally determines the start curve for both the offset curve planner and the section plane planner.

Note that if a section plane is orthogonal to the target surface at all points on the intersection curve, then the intersection curve is a geodesic. In Section IV-B, we tried to pick a section plane that is "as orthogonal as possible" to the target surface by restricting the section normals to $\mathcal{N}_{\text{uni}}$. Therefore, for such section planes we can say that the intersection curve of the surface and the section plane is close to being a geodesic. Then, within reasonable limits, we can apply the Gaussian divider result from Section III-B for choice of start curve, where the start curve is defined by intersection of the section plane with normal $\mathbf{N}^*$ and the target surface.

We define the optimal start curve α^* as the intersection curve of the surface and the plane with normal $\mathbf{N}^*$, such that α^* is a Gaussian curvature divider. That is, if $P_k(N)$ denotes the plane $\langle N, x\rangle = k$ and if α splits surface S into regions ϕ^- and ϕ^+, the optimal start curve for the offset curve planner is

$$\alpha^* = P_k(\mathbf{N}^*) \cap S \text{ s.t. } \int_{\phi^-} K = \int_{\phi^+} K. \qquad (16)$$

The existence of α^* is guaranteed by the fact that for a given $\mathbf{N}^*$ a section plane $P_k(\mathbf{N}^*)$ exists such that the intersection of the section plane and the target surface is a Gaussian curvature divider. The proof follows by application of the intermediate value theorem to the continuous function $f = (\int_{\phi^-} K - \int_{\phi^+} K)$ with the fact that $\int_S K$ has a finite value. Clearly, from Equation 16, α^* is close to being a geodesic Gaussian curvature divider; thus results from Section III suggest that the coverage path constructed using α^* will satisfy the uniformity criterion. Simultaneously, α^* is constructed using the section plane normal $\mathbf{N}^*$ that is cycle time optimal. Thus, α^* simultaneously optimizes the deposition uniformity and cycle time.

For the section plane planner, the intersection curve of any plane with normal $\mathbf{N}^*$ can be viewed as the optimal start curve. The curve α^* by its definition is such a curve, and selecting α^* as the optimal start curve resolves the ambiguity of selecting the positions (distance from origin) of the equidistant series of section planes. Thus, α^* gives the location of the optimal start curve both for the offset curve planner and the section plane planner.

V. Simulation Results

Here, we compare simulation results for coverage paths constructed using our method and a method based on the Gauss Map (Smith *et al.* [8]). Our method selects the optimum orientation of the section plane defining the start curve as described in this text, whereas the *Gauss Map Modified (GMM)* selects the optimum orientation of the section plane as the center of largest circle inscribed in the complement of the symmetrized Gauss map. For a meaningful comparison, both methods utilize offset curve planner for coverage path construction, where the orthogonal curves (used for offsetting procedure) are obtained by intersecting planes orthogonal to the start curve. This procedure of offsetting closely approximates the offsetting procedure that uses geodesics as orthogonal curves. Our method as well as the GMM method selects the start curve from the family of Gaussian curvature dividers for corresponding orientations of section planes.

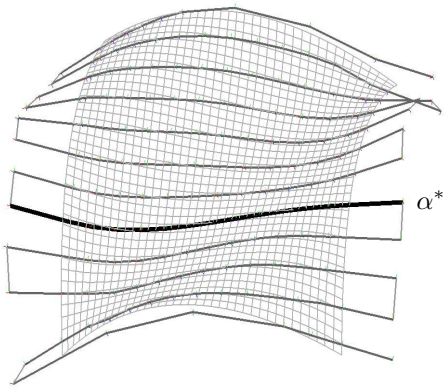

Fig. 8. The thick dark curve (α^*) is the Gaussian curvature divider for optimal normal $\mathbf{N}^*$. We choose α^* as the start curve.

The test surfaces used by Smith *et al.* [8] are very small compared to the width of spray gun deposition pattern. To have realistic paint deposition scenarios, we scale surface #2 described in [8] by a factor of $\frac{1000}{2.54}$ (see Figure 8). Using the deposition model described in [7], we simulate the paint deposition process. In Table I, we compare our method to GMM method. Our method yields a 20% relative improvement for the deposition uniformity, where we measure the uniformity in terms of normalized standard deviation of paint deposition. Also, there is a relative improvement of 16.66% in cycle time (measured in terms of number of turns). We also compare the two approaches for more realistic auto body surfaces, e.g., a surface approximating the shape of Ford Crown Victoria front side fender. For this fender-resembling surface, our method yields normalized standard deviation for paint equal to 17.16%, where the resultant coverage path is free from self-intersections. The coverage path constructed using the GMM method has self-intersections and as a result the normalized standard deviation of paint deposition for this coverage path is high at 45.19%. For this fender approximation surface, our method gives the number of turns in the coverage path equal to 6, where as for the GMM method it is 9.

VI. Conclusion

The results of our analysis show that the choice of a start curve impacts the uniformity of material deposition

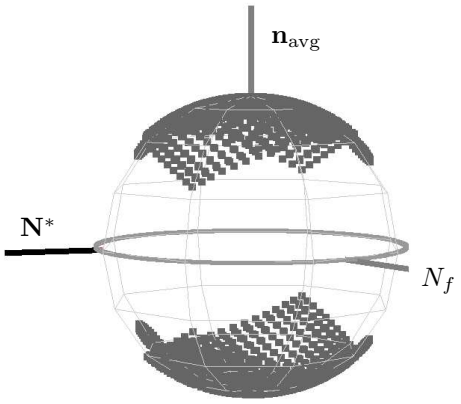

Fig. 9. Symmetrized Gauss Map for surface shown in Figure 8. $\mathbf{n}_{\text{avg}}$ is the average surface normal, optimal section normal by our approach is $\mathbf{N}^*$, whereas by GMM it is N_f.

Test Surface	Our approach		GMM method	
	Std dev	Turns	Std dev	Turns
Surf #2	11.34%	12	13.67%	14
CV fender app	17.16%	6	45.19%	9

TABLE I
COMPARISON OF OUR METHOD TO GMM APPROACH

and the system's cycle time. By making a recourse to basic differential geometry, particularly the Gauss-Bonnet theorem, we arrive at an important result that the geodesic curvature of the offset curve is minimized by using a start curve that is a geodesic Gaussian curvature divider. The minimization of geodesic curvature of the offset curves is critical for ensuring uniform coverage, and thus geodesic Gaussian curvature dividers are a key step in drastically reducing the search space of start curves that meet the uniformity goal. Cycle time optimization over the family of geodesic Gaussian curvature dividers helps us to select a start curve that meets the uniformity goal as well as optimizes cycle time criterion.

VII. ACKNOWLEDGMENT

This work was supported by the National Science Foundation and the Ford Motor Company through grant IIS-9987972. The authors gratefully acknowledge the input provided by David C. Conner and Aaron Greenfield at Carnegie Mellon University and by Dr. Jacob Braslaw, our collaborator, at the Ford Motor Company.

VIII. REFERENCES

[1] K. Suresh and D.C.H. Yang. Constant Scallop Height Mechining of Free-form Surfaces. *Journal of Engineering for Industry*, 116:253–259, May 1994.

[2] R. Sarma and D. Dutta. The Geometry and Generation of NC Tool Paths. *Journal of Memchanical Design*, 119, June 1997.

[3] Suk-Hwan Suh, In-Kee Woo, and Sung-Kee Noh. Development of An Automated Trajectory Planning System (ATPS) for Spray Painting Robots. In *IEEE Int'l. Conf. on Robotics and Automation*, Sacremento, California, USA, April 1991.

[4] M. A. Sahir and Tuna Balkan. Process Modeling, Simulation, and Paint Thickness Measurement for Robotic Spray Painting. *Journal of Robotic Systems*, Vol. 17(9), 2000.

[5] Naoki Asakawa and Yoshimi Takeuchi. Teachless Spray-Painting of Sculptured Surface by an Industrial Robot. In *IEEE Int'l. Conf. on Robotics and Automation*, Albuquerque, New Mexico, USA, April 1997.

[6] Weihua Sheng, Ning Xi, Mumin Song, Yifan Chen, and Perry MacNeille. Automated CAD-Guided Robot Path Planning for Spray Painting of Compound Surfaces. In *IEEE/RSJ Int'l. Conf. on Intelligent Robots and Systems*, 2000.

[7] David C. Conner, Prasad N. Atkar, Alfred A. Rizzi, and Howie Choset. Development of Deposition Models for Paint Application on Surfaces Embedded in $I\!R^3$ for Use in Automated Path Planning. In *IEEE/RSJ Int'l. Conf. on Intelligent Robots and Systems*, Lausanne, Switzerland, 2002.

[8] Tait S. Smith, Rida T. Farouki, Mohammad al Kandari, and Helmut Pottman. Optimal Slicing of free-form surfaces. *Computer Aided Geometric Design*, 19, 2002.

[9] Wesley H. Huang. Optimal Line-sweep-based Decompositions for Coverage Algorithms. In *IEEE Int'l. Conf. on Robotics and Automation*, Seoul, Korea, May 2001.

[10] Thomas Rausch, Franz-Erich Wolter, and Oliver Sniehotta. Computation of Medial Curves on Surfaces. *The Mathematics of Surfaces VII*, Information Geometers, 1997.

[11] J.A. Thorpe. *Elementary Topics in Differential Geometry*. Springer-Verlag., New York, NY, 1979.